ACS APPLIED MATERIALS & INTERFACES

Research Article

www.acsami.org

Preparation of Novel Three-Dimensional NiO/Ultrathin Derived Graphene Hybrid for Supercapacitor Applications

ChunHui Wu,[†] SiXu Deng,[†] Hao Wang,*[,†,‡] YuXiu Sun,[†] JingBing Liu,[†] and Hui Yan[†,‡]

[†]The College of Materials Science and Engineering, Beijing University of Technology, Beijing 100124, P.R. China

[‡]Chengdu Green Energy and Green Manufacturing Technology R&D Centre, Shuangliu, Chengdu 610207, P.R. China

ABSTRACT: A new type of three-dimensional (3D) NiO/ultrathin derived graphene (UDG) hybrid on commercial Ni foam (NF) for a binder-free pseudocapacitor electrode is presented. NiO nanoflakes are in situ grown by a chemical bath deposition (CBD) technique on the free-standing 3D UDG/NF scaffold, which is first prepared by a simple nanocasting process consisting of hydrothermal reaction and subsequent thermal transformation. The 3D UDG/NF scaffold with interconnected network affords a high conductivity due to the high graphitization degree and efficiently facilitates the electron transport to NiO. Moreover, the 3D NiO/UDG/NF hybrid allows for a thinner 3D active material layer under the same loading density, which could shorten the diffusion paths of ions. The NiO/UDG/NF hybrid is directly used as a binder-free supercapacitor electrode, which exhibited significantly improved supercapacitor performance compared to the bare CBD prepared NiO/NF electrode.

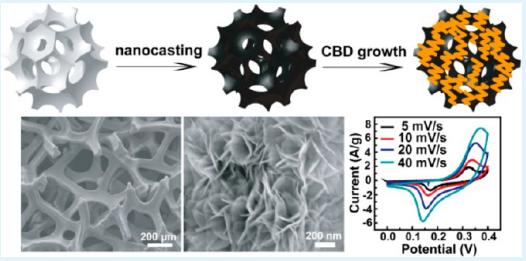

KEYWORDS: *NiO, 3D derived graphene, supercapacitor, binder free, scaffold, nanoflake*

1. INTRODUCTION

Supercapacitors (also known as electrochemical capacitors) with high power density and long lifespan are of interest in energy storage applications such as uninterruptible back-up power supplies, hybrid electronic vehicles, and renewable energy systems.[1−3] RuO_2 is widely recognized as the best electrode material for pseudocapacitors.[4] However, apart from being toxic, RuO_2 is quite expensive for extensive commercial application. As an inexpensive alternative material with good capacitive characteristics, NiO is of particular interest owing to its easy availability, cost effectiveness, and good pseudocapacitive behavior.[5−7] However, they often suffer from poor rate capability and reversibility because redox kinetics is limited by the rates of ion diffusion and electron transfer. In attempts to improve the electrochemical performance of NiO-based electrodes, NiO nanostructures with high surface area as well as NiO anchoring onto highly conductive substrates such as conducting polymers, carbon nanotubes, and graphene were mostly researched.[8−11]

Among these substrates, graphene has attracted tremendous attention for its unique properties over other carbon nanomaterials, including superior electrical conductivity, high specific surface area, and chemical stability.[3,12,13] Recently, three-dimensional (3D) graphene, which provides a low density and free-standing 3D interconnected network with high electrical conductivity, has been researched in many areas.[14−16] It is also an ideal candidate to serve as the scaffold for fabrication of adsorbents, catalyst supports, monolithic composite electrodes, and so on. So far, various "bottom up" approaches toward the 3D architecture of graphene have been developed, such as chemical vapor deposition (CVD) and self-assembly of graphene oxide.[17−20] Cheng et al. developed a 3D foam-like graphene with a very high electrical conductivity by a general template-directed CVD technique.[17] Shi et al. reported a 3D mechanically strong, electrically conductive, and thermally stable self-assembled graphene hydrogel (SGH) with a high specific capacitance, which was prepared from graphene oxide by a one-step hydrothermal method.[20] Yun et al. fabricated assembled embossed chemically modified graphene film by using polystyrene colloidal particles as a sacrificial template and explored its use in supercapacitor electrodes.[21] However, 3D graphene is still prohibitively expensive for large-scale manufacturing of graphene-based bulk materials. Nanocasting, as a "top down" strategy, is widely used for preparing carbon materials on special templates.[22−24] Normally, special organics (e.g., phenolic resols and poly(methyl methacrylate)) as the carbon source and catalysts (e.g., nickel, iron, and manganese) were used to realize a low transformation temperature from precursor to carbon materials.[25−27] The nanocasting process is most commonly used for preparation of various mesoporous carbon structures. However, it is rarely employed to the synthesis of 3D graphene with continuous microstructured networks.

In this work, we prepared a novel 3D NiO/ultrathin derived graphene (UDG) hybrid on Ni foam (NF) by a two-step approach. The 3D UDG/NF scaffold was first prepared by a simple nanocasting process, and then NiO nanoflakes were in situ grown on the scaffold via a chemical bath deposition

Received: October 23, 2013
Accepted: January 6, 2014
Published: January 6, 2014

 © 2014 American Chemical Society

Scheme 1. Synthetic Scheme of the NiO/UDG/NF Hybrid

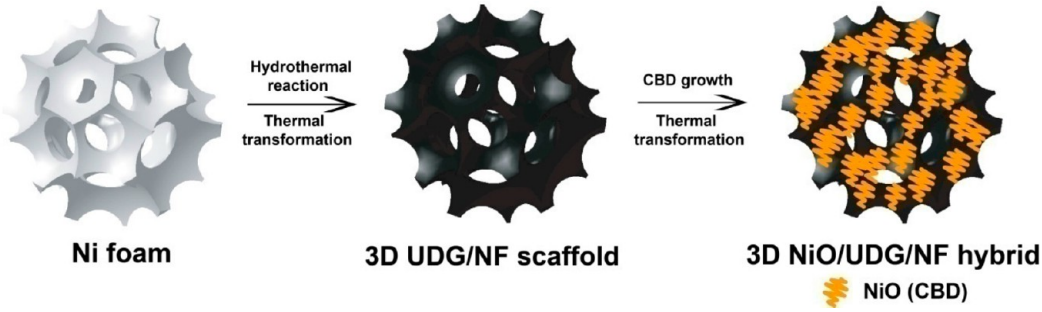

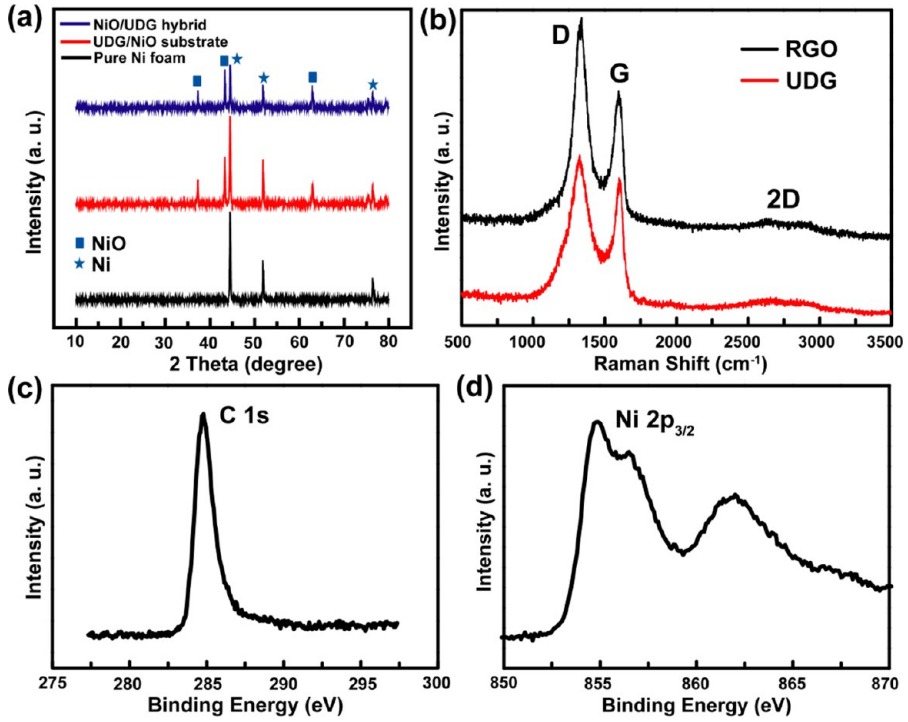

Figure 1. (a) XRD patterns of pure Ni foam, UDG/NF scaffold, and NiO/UDG/NF hybrid. (b) Raman spectra of RGO and UDG. (c, d) XPS spectra of C 1s and Ni 2p of UDG/NF.

(CBD) technique. The resulting NiO/UDG/NF hybrid was directly used as a binder-free supercapacitor electrode, in view that the generally used polymer binder may increase resistance and reduce capacitance. The 3D NiO/UDG/NF hybrid electrode exhibits significant improved supercapacitor performance compared to the bare CBD prepared NiO/NF electrode.

2. EXPERIMENTAL SECTION

2.1. Chemicals. Pluronic F127 ($PEO_{106}PPO_{70}PEO_{106}$, M_w = 12 600) was provided by Aldrich (U.S.A). Phenol and formaldehyde (37.0−40.0% aqueous solution) were from Tianjin Fuchen Chemical Reagent Company (China). Ni foam (thickness: 1.7 mm, areal density: 200 ± 20 g/m^2) was from Heze Tianyu Technology Development Co., Ltd. (China). Sodium hydroxide (96.0%), potassium peroxydisulfate ($K_2S_2O_8$), nickel sulfate ($NiSO_4$), and concentrated ammonia (25% aqueous solution) were purchased from Beijing Chemical Reagent Company (China). All chemicals were used as received without any further purification. All aqueous solutions were prepared using ultrapure water (Milli-Q, Millipore).

2.2. Sample Preparation. *2.2.1. Synthesis of the 3D UDG/NF Scaffold.* The preparation process was shown in Scheme 1. In a typical preparation process, low-molecular-weight phenolic resols (LPRs) were first synthesized through a base-catalyzed process.[25,28] An amount of 1.2 g of phenol was melted at 40 °C in a flask and mixed with 4.2 mL of formaldehyde solution (37%) and 30 mL of 0.1 M NaOH aqueous solution. Then, the mixture was stirred at 70 °C for 0.5 h to obtain low-molecular-weight phenolic resols. After that, 30 mL of Pluronic F127 (1.92 g) aqueous solution was added into the mixture and stirred for 4 h. Afterward, 100 mL of H_2O was added to dilute the solution, and the mixture was further stirred at 69 °C for over 12 h until deposition was observed. Second, the Ni foam (1× 1.5 cm) was put into an autoclave (100 mL volume) with 25 mL of the as-prepared monomicelle solution and kept still for 3 h for a sufficient contact between the Ni foam and solution. After that, 50 mL of H_2O was added to dilute the solution. Hydrothermal treatment was then carried out in an oven at 130 °C for 20 h. After cooling to room temperature, the Ni foam was taken out from the autoclave, washed with water, and cleaned with wipe paper several times. Then, it was dried at 45 °C for 2 days. After that, it was carbonized at 350 °C for 3 h in nitrogen and further graphitized at 800 °C for 2 h in nitrogen. The obtained product was a NiO/NF scaffold.

2.2.2. Chemical Bath Deposition of NiO Nanoflakes on the UDG/NF Scaffold. The NiO nanoflakes were prepared by chemical bath deposition from the previous reports.[29] Specifically, 30 mL of 0.25 M $K_2S_2O_8$, 40 mL of 1 M $NiSO_4$, 10 mL of concentrated ammonia (25% aqueous solution), and 20 mL of deionized water were mixed for the synthesis of NiO nanoflakes. After deposition on the NiO/UDG

substrate, the films were calcined in a tube furnace at 350 °C for 2 h in flowing nitrogen. The obtained product on the Ni foam was a NiO/UDG/NF hybrid electrode.

2.3. Characterization. X-ray diffraction (XRD) patterns were recorded on a Shimadzu XRD diffractometer with Cu Kα. Raman spectroscopy was performed using a Renishaw inVia Raman microscope with an excitation wavelength of 633 nm provided by an argon laser. The X-ray photoelectron spectroscopy (XPS) measurements were performed using an ESCALAB 250 XPS using an Al K_α (1486.6 eV) X-ray source. To exclude the influence from surface-absorbed oxygen and carbon, Ar^+ ion (3 keV) etching for 3 min was performed before collecting the X-ray generated electrons. All binding energies for the XPS spectra were calibrated by setting C 1s at 284.6 eV. Scanning electron microscopy (SEM) and element mapping images were collected using a Hitachi S4800 field emission scanning electron microscopy (FESEM). Transmission electron microscopy (TEM) and high-resolution transmission electron microscopy (HRTEM) images were collected on a JEM-2100 with an acceleration voltage of 200 kV.

2.4. Electrochemical Measurements. Cyclic voltammetry (CV), chronopotentiometry (CP), and electrochemical impedance spectroscopy (EIS) measurements were carried out using a conventional three-electrode configuration on a solartron electrochemical workstation. The 3D NiO/UDG/NF electrode (area of 1 cm × 1.5 cm) with a mass loading of 0.01 g/cm^2 NiO/UDG hybrid was directly used as the working electrode, and platinum foil (1 cm × 1 cm) and a saturated calomel electrode (SCE) were used as the counter and reference electrodes. All experiments were carried out in freshly prepared 5.0 M aqueous KOH electrolyte. The EIS measurements were carried out in the frequency ranges from 100 kHz to 0.01 Hz at open-circuit potential with AC perturbation amplitude of 5 mV.

3. RESULTS AND DISCUSSION

3.1. Material Characterization. Figure 1a showed the XRD patterns of pure NF, UDG/NF scaffold, and NiO/UDG/NF hybrid. As the 3D support for the UDG substrate and NiO/UDG hybrid, Ni foam showed three strong peaks at 44.4°, 51.9°, and 76.4° in the three samples. The diffraction peaks at 37.2°, 43.2°, and 62.8° can be well assigned to the cubic NiO phase (JCPDS 4-0835). The pattern of NiO on the UDG/NF scaffold was mainly because Ni foam was partially converted to $Ni(OH)_2$ under the hydrothermal reaction environment, following with the change into NiO after thermal treatment. After CBD growth of NiO nanoflakes, the intensity ratio of the main peak of NiO (43.2°) to Ni (44.4°) increased dramatically. Apart from the XRD peaks of Ni and NiO shown in Figure 1a, no diffraction peak that belonged to the UDG was observed. This phenomenon is probably due to the fact that the signal of UDG is overlapped by Ni and NiO. To further demonstrate this hypothesis, we tested the Raman spectrum of UDG on NF in Figure 1b. In addition, because reduced graphene oxide (RGO) is a widely recognized graphene structure, we compared the Raman spectrum of RGO which was prepared through a direct reduction of graphene oxide (GO) by hydrazine[30] and that of UDG in our work to help us illustrate the structure and layers of UDG. As is well-known, Raman scattering is strongly sensitive to the electronic structure, and it has proved to be an essential tool to characterize graphite and graphene materials. We found that the Raman spectrum of UDG exhibited a very similar spectrum with that of RGO. The Raman band at around 1585 cm^{-1} (the G band) can be assigned to the E_{2g} phonon of C sp^2 atoms, which is mainly due to the existence of carbon atoms of the graphite phase. The peak at around 1346 cm^{-1} (the D band) is derived from a breathing mode of κ-point phonons of A_{1g} symmetry, which is related to the considerable bond disorder such as the presence of five- and seven-membered rings.[31,32] As the overtone of the D band, the 2D band at around 2700 cm^{-1} is attributed to double resonance transitions resulting in production of two phonons with opposite momentum. The shape of the 2D band has been correlated with the number of graphene layers. In Figure 1b, we could see a weak and broad 2D splitting peak in both UDG and RGO, which was an indication of disorder and coupling of the stacked multilayers of graphene sheets.[33,34] From the Raman results, we ensured the multilayered graphene structure of the UDG on the Ni foam template in our work. Furthermore, to investigate the electronic state of elements in compounds, we tested the XPS spectra of UDG/NF which were shown in Figure 1c and 1d. The UDG/NF sample had a peak at 284.8 eV in the C 1s spectrum, which can be assigned to C−H, C−C, $(CH_2)_n$, and C═C bonds that are characteristic of graphite/graphene.[22,35] The XPS pattern of UDG/NF also showed the binding energy of Ni $2p_{3/2}$ at 851.6 eV, typical of the Ni phase of NiO. These results are consistent with the XRD and Raman results. From the above results, we could see that both the use of low-molecular-weight phenolic resols as the amorphous carbon source and Ni as the graphitization catalyst play important roles in decreasing the graphitization temperature. The resulting 3D UDG/NF with a high graphitization degree provides a good 3D contact surface and could act as a highly conductive scaffold for deposition of NiO.

Figure 2 showed the typical morphologies of pure NF, the 3D UDG/NF scaffold, and UDG through FESEM (a−c), TEM

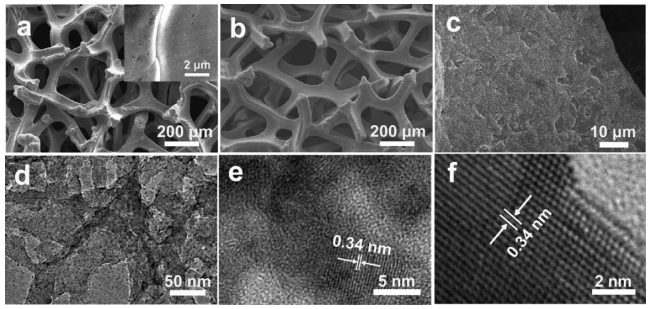

Figure 2. (a) Low- and high-resolution (inset) SEM images of pure Ni foam. (b) SEM image of the UDG/NF scaffold. (c) High-resolution SEM image of the 3D UDG/NF scaffold. (d) TEM image of UDG. (e, f) HRTEM images of UDG.

(d), and HRTEM (e,f) images. In Figure 2a, the pure NF exhibited a three-dimensional cross-linked structure with considerable grids on its surface, and a bright smooth surface could be seen in the high-resolution image (inset of Figure 2a). After the uniform growth of UDG, the surface morphology changed dramatically, which we could see from the low- and high-resolution images in Figure 2b and 2c. To investigate the morphology of UDG, we examined the TEM image of UDG by etching away Ni and NiO by 3 M HCl at 80 °C. Ultrathin morphology of the derived graphene could be seen obviously in Figure 2d. Moreover, UDG was characterized by the HRTEM at two sites on the sample (Figure 2e and 2f). We could see that the HRTEM images showed a high crystallinity with lattice-resolved fringes. The spacing between adjacent graphene planes was measured as 0.34 nm, corresponding to the (002) planes of graphene.

To further realize and investigate the microstructure and elemental distribution of the 3D UDG/NF scaffold, scanning electron microscopic elemental mapping was employed. A SEM

image and the corresponding elemental mapping images of carbon, oxygen, and nickel were shown in Figure 3. The

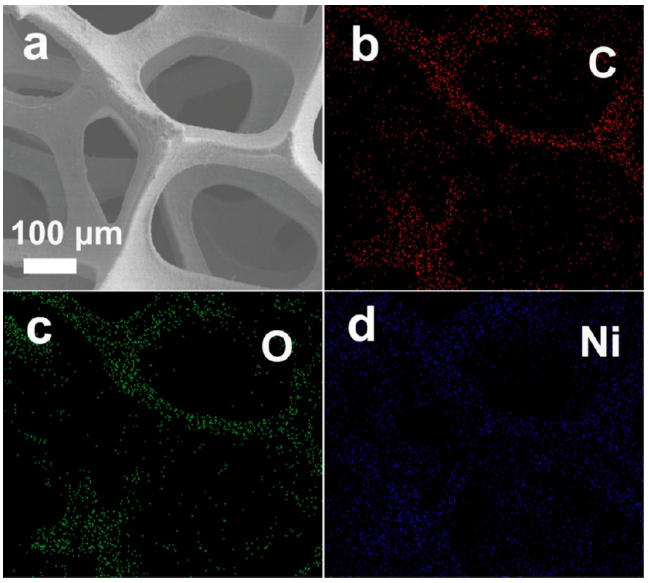

Figure 3. SEM image of (a) the UDG/NF scaffold on Ni foam and elemental mapping images of (b) carbon, (c) oxygen, and (d) nickel on the UDG/NF scaffold.

uniform and continuous distribution of carbon and nickel elements on UDG/NF confirmed the homogeneous growth of UDG on the whole 3D macroporous frameworks. In addition, the existence of an oxygen element was attributed to the small amount of NiO converted from Ni foam, which was identical with the XRD results.

Figure 4 showed the SEM images of the 3D NiO/UDG/NF hybrid. In Figure 4b, we could see a uniform growth of NiO nanoflakes on the 3D UDG/NF scaffold (Figure 4a), resulting in the formation of a 3D NiO/UDG/NF hybrid. Figure 4c showed the morphology of urchin-like NiO with a diameter

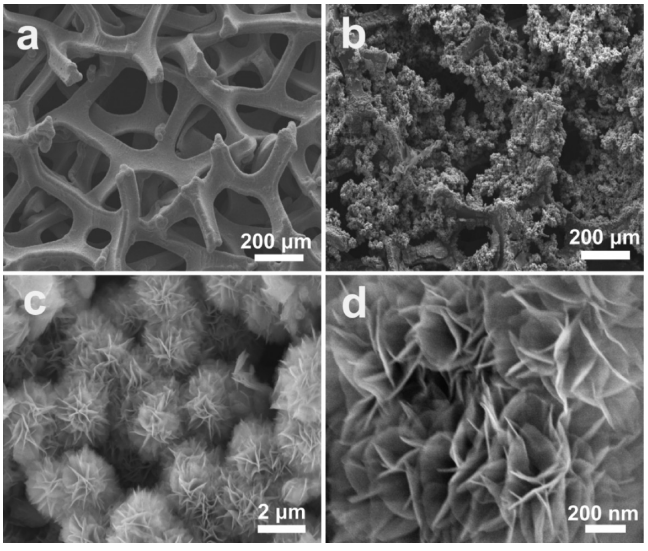

Figure 4. SEM images of (a) 3D UDG/NF scaffold and (b) 3D NiO/UDG/NF hybrid after CBD growth of NiO nanoflakes. (c,d) Low- and high-resolution SEM images of NiO nanoflakes grown by the CBD technique.

around 1 μm through the CBD method. Careful observation (Figure 4d) can find that the urchin-like nanostructure consisted of uniform nanoflakes. Combined with the above results, it suggests that the 3D UDG/NF scaffold with a high graphitization degree and continuous 3D reticulation not only provides 3D surface contact for the growth of NiO or other active materials but also possesses a high conductivity due to the presence of UDG, which may enable good pseudocapacity of the 3D NiO/UDG/NF hybrid.[36,37]

3.2. Electrochemical Characterization. Using the NiO/UDG/NF hybrid electrode as a free-standing binder-free working electrode, we then analyzed their electrochemical capacitance performance with 5.0 M KOH as electrolyte. To investigate the difference of capacitance performance when using our prepared 3D UDG/NF scaffold, we prepared NiO nanostructure on NF (NiO/NF) as a working electrode for comparison through the CBD technique using the same mixed precursor solution as for the NiO/UDG/NF hybrid. Figure 5a

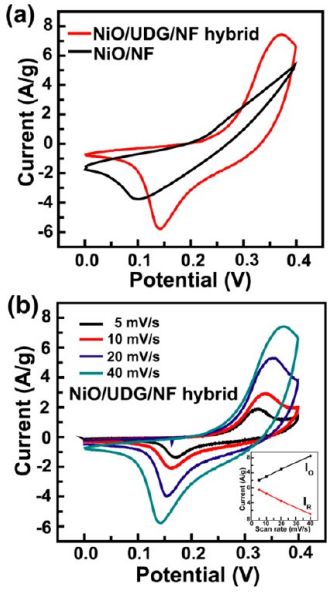

Figure 5. (a) Comparison of cyclic voltammograms of the NiO/UDG/NF hybrid and NiO/NF electrode at a scan rate of 40 mV/s. (b) CV curves of the NiO/UDG/NF hybrid at different scan rates and linear response of the peak current intensity with the scan rate (inset).

showed the CV curves of the NiO/UDG/NF hybrid electrode and NiO/NF electrode at a scan rate of 40 mV/s in the potential range of 0−0.4 V vs SCE. From the CV curves in Figure 5a, it can be observed that the capacitance is mainly based on the redox reaction because the shape of the CVs is distinguished from that of electric double-layer capacitance, which is normally close to an ideal rectangular. During the scans, no reduction peak could be seen in the CV curve of the NiO/NF electrode due to the poor conductivity of NiO. In contrast, a pair of nearly reversible reduction and oxidation peaks were observed in the CV curve of the NiO/UDG/NF hybrid electrode, in which nickel hydroxide (NiOOH) is formed at the surface of the nickel during the cycling in the KOH aqueous solution. The respective reduction and oxidation peaks correspond to the following charge−discharge phenomena

$$NiO + OH^- \leftrightarrow NiOOH + e^- \quad (1)$$

dx.doi.org/10.1021/am404691w | ACS Appl. Mater. Interfaces 2014, 6, 1106−1112

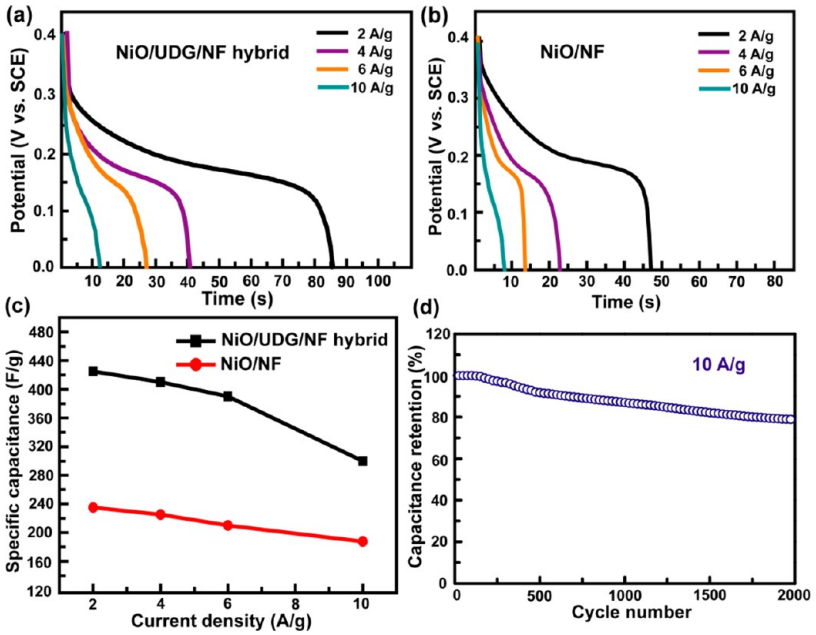

Figure 6. Discharge curves of the NiO/UDG/NF hybrid (a) and NiO/NF (b) electrode at different current densities. (c) Specific capacitance as a function of currents for the NiO/UDG/NF hybrid and NiO/NF electrode. (d) Cycling performance of the NiO/UDG/NF hybrid electrode at a current density of 10 A/g.

From the above results, we could see that the presence of the UDG substrate plays an important role in improving the electron transfer rate and decreasing the ohmic resistance of the electrolyte diffusion in the electrode during the redox reactions. The CV responses of the NiO/UDG/NF hybrid electrode performed at different scan rates (5−40 mV s^{-1}) were shown in Figure 5b. A slightly positive shift of the oxidation peak potential and a negative shift of the reduction peak potential are due to the electric polarization and irreversible reactions at a higher scan rate.[38] The linear response of the peak current intensity with the scan rate (inset of Figure 5b) is also an indication of the fast electronic and ionic transport rates.

Figure 6 displayed a set of galvanostatic discharge curves in the first cycle at current densities of 2, 4, 6, and 10 A/g. Specific capacitance values of the NiO/UDG/NF hybrid electrode and NiO/NF electrode had been calculated from chronopotentiometric measurements at applied current densities (i), active mass of the sample (m), and the discharge slope of the chronopotentiometric discharge curve (dV/dt), using the equation

$$Cs = \frac{i}{[m(dV/dt)]}$$

The specific capacitance values of the NiO/UDG/NF hybrid electrode at different current densities of 2, 4, 6, and 10 A g^{-1} were found to be 425, 410, 390, and 300 F/g, respectively. Similarly, the specific capacitance values for the NiO/NF electrode at the same current densities were found to be 235, 225, 210, and 187.5 F/g, respectively (Figure 6c). Compared to the NiO/NF electrode, the capacitance of the NiO/UDG/NF hybrid electrode was much larger. The reasons may be summarized as follows: (1) the introduction of a 3D highly conductive UDG/NF scaffold provides a good 3D contact surface for NiO and can efficiently improve the electron transfer rate to NiO; (2) the urchin-like nanostructure of NiO growth by CBD together with the 3D structure of the NiO/UDG/NF hybrid provide a large electrode/electrolyte contact area; (3) the 3D NiO/UDG/NF hybrid allows for a thinner 3D active material layer under the same loading density, which could shorten the diffusion paths of ions; (4) the direct use of the free-standing 3D NiO/UDG/NF hybrid as the supercapacitor electrode avoids the use of a nonconducting polymer binder. Figure 6d showed the specific capacitance variation for the NiO/UDG/NF hybrid electrode as a function of cycle number at a current density of 10 A/g within a voltage range between 0 and 0.4 V. There was about 21% specific capacitance loss after 2000 cycles.

Electrochemical impedance spectroscopy (EIS) is a simple yet powerful chemical analysis technique for conductivity measurement. To study the electrochemical response of the NiO/UDG/NF hybrid electrode, EIS was performed with a frequency range of 100 kHz to 0.01 Hz at an AC perturbation amplitude of 5 mV. The Nyquist plots of NiO/UDG/NF, NiO/NF, and UDG/NF were shown in Figure 7. The fitting

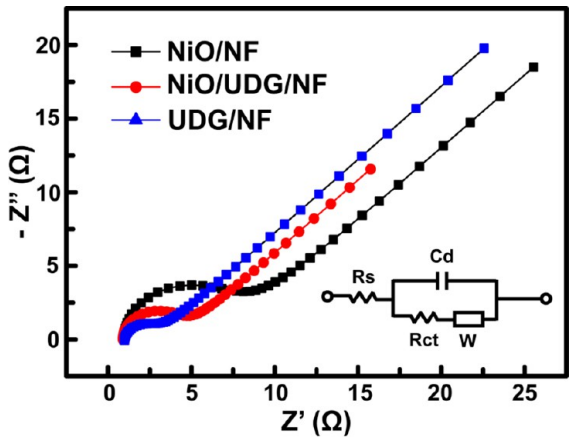

Figure 7. Nyquist plots of NiO/UDG/NF, NiO/NF, and UDG/NF electrodes. Inset showed the electrical equivalent circuit used for fitting impedance spectra.

dx.doi.org/10.1021/am404691w | ACS Appl. Mater. Interfaces 2014, 6, 1106−1112

curve, followed by Randles equivalent circuit, was also obtained and shown in the bottom right of Figure 7. Each plot was characterized by a semicircle in the high-frequency region and a straight line in the low-frequency region. The diameter of the semicircle corresponded to the charge transfer resistance (R_{ct}) for the redox reaction at the electrode/electrolyte interface. The straight line with an angle at almost 45° with the real axis indicated the presence of Warburg resistance which is attributed to the diffusion transfer limitation of charged ions in the presence of aggregated NiO nanoflakes and UDG. It is well accepted that a larger semicircle means a larger charge-transfer resistance, and a steeper slope signifies a lower ion-diffusion rate. The Nyquist plots of three samples in Figure 7 clearly showed that the charge transfer resistance decreased and the ion diffusion rate increased for the NiO/UDG/NF hybrid electrode when compared with the NiO/NF electrode, while UDG/NF exhibited the lowest charge transfer resistance. This improved electrochemical performance can be attributed to the introduction of UDG into the hybrid film, leading to improved conductivity of the composite and a decrease in the internal resistance of the electrode.

4. CONCLUSION

In summary, we successfully developed a new type of NiO/UDG/NF hybrid as the binder-free supercapacitor electrode through a two-step approach, in which the 3D UDG/NF scaffold was prepared via a simple nanocasting process from an amorphous carbon source. The as-obtained hybrid materials were characterized by XRD, Raman, XPS, SEM, and TEM measurements. The NiO/UDG/NF hybrid electrode exhibited improved pseudocapacitive performance compared to the NiO/NF electrode, which showed higher capacitances of 425 and 300 F/g at 2 and 10 A/g, respectively. It also showed good capacity retention of ca. 90% after 500 charge−discharge cycles. The introduction of the 3D UDG/NF scaffold can greatly improve the electron transfer rate and the electrochemical activity of the reversible reaction of Ni^{II} and Ni^{III}. The binder-free 3D NiO/UDG/NF hybrid electrode provides a good 3D electrode/electrolyte contact and short ion diffusion paths. In our view, the Ni foam template-directed nanocasting prepared 3D UDG/NF scaffold affords a low-temperature and large-scale preparation of 3D graphene material from an amorphous carbon source and an interconnected 3D network with good electron conductivity. The 3D UDG/NF scaffold also has potential applications in other research areas such as electronics and sensors.

AUTHOR INFORMATION

Corresponding Author

*E-mail: haowang@bjut.edu.cn. Tel.: +86-10-6739-2733.

Notes

The authors declare no competing financial interest.

ACKNOWLEDGMENTS

This work was supported by the Foundation on the Creative Research Team Construction Promotion Project of Beijing Municipal Institutions, 2013 Annual Rixin Training Support Project of Beijing University of Technology, and the Doctoral Fund of Innovation of Beijing University of Technology.

REFERENCES

(1) Simon, P.; Gogotsi, Y. *Nat. Mater.* **2008**, *7*, 845−854.
(2) Kötz, R.; Carlen, M. *Electrochim. Acta* **2000**, *45*, 2483−2498.
(3) Pandolfo, A. G.; Hollenkamp, A. F. *J. Power Sources* **2006**, *157*, 11−27.
(4) Hu, C.-C.; Chang, K.-H.; Lin, M.-C.; Wu, Y.-T. *Nano Lett.* **2006**, *6*, 2690−2695.
(5) Liu, X.-M.; Zhang, X.-G.; Fu, S.-Y. *Mater. Res. Bull.* **2006**, *41*, 620−627.
(6) Lu, Q.; Lattanzi, M. W.; Chen, Y.; Kou, X.; Li, W.; Fan, X.; Unruh, K. M.; Chen, J. G.; Xiao, J. Q. *Angew. Chem., Int. Ed.* **2011**, *50*, 6847−6850.
(7) Xu, J.; Gao, L.; Cao, J.; Wang, W.; Chen, Z. *J. Solid State Electrochem.* **2011**, *15*, 2005−2011.
(8) Ge, C.; Hou, Z.; He, B.; Zeng, F.; Cao, J.; Liu, Y.; Kuang, Y. *J. Sol-Gel Sci. Technol.* **2012**, *63*, 146−152.
(9) Lee, J. W.; Ahn, T.; Kim, J. H.; Ko, J. M.; Kim, J.-D. *Electrochim. Acta* **2011**, *56*, 4849−4857.
(10) Lin, P.; She, Q.; Hong, B.; Liu, X.; Shi, Y.; Shi, Z.; Zheng, M.; Dong, Q. *J. Electrochem. Soc.* **2010**, *157*, A818−A823.
(11) Tao, B.; Zhang, J.; Miao, F.; Hui, S.; Wan, L. *Electrochim. Acta* **2010**, *55*, 5258−5262.
(12) Allen, M. J.; Tung, V. C.; Kaner, R. B. *Chem. Rev.* **2009**, *110*, 132−145.
(13) Wang, Y.; Shi, Z.; Huang, Y.; Ma, Y.; Wang, C.; Chen, M.; Chen, Y. *J. Phys. Chem. C* **2009**, *113*, 13103−13107.
(14) Wu, Z.-S.; Sun, Y.; Tan, Y.-Z.; Yang, S.; Feng, X.; Müllen, K. *J. Am. Chem. Soc.* **2012**, *134*, 19532−19535.
(15) Jiang, H.; Lee, P. S.; Li, C. *Energy Environ. Sci.* **2013**, *6*, 41−53.
(16) Zhang, H.; Zhang, X.; Zhang, D.; Sun, X.; Lin, H.; Wang, C.; Ma, Y. *J. Phys. Chem. B* **2012**, *117*, 1616−1627.
(17) Chen, Z.; Ren, W.; Gao, L.; Liu, B.; Pei, S.; Cheng, H.-M. *Nat. Mater.* **2011**, *10*, 424−428.
(18) Ji, J.; Zhang, L. L.; Ji, H.; Li, Y.; Zhao, X.; Bai, X.; Fan, X.; Zhang, F.; Ruoff, R. S. *ACS Nano* **2013**, *7*, 6237−6243.
(19) Bello, A.; Makgopa, K.; Fabiane, M.; Dodoo-Ahrin, D.; Ozoemena, K. I.; Manyala, N. *J. Mater. Sci.* **2013**, *48*, 6707−6712.
(20) Xu, Y.; Sheng, K.; Li, C.; Shi, G. *ACS Nano* **2010**, *4*, 4324−4330.
(21) Choi, B. G.; Yang, M.; Hong, W. H.; Choi, J. W.; Huh, Y. S. *ACS Nano* **2012**, *6*, 4020−4028.
(22) Sun, Z.; Yan, Z.; Yao, J.; Beitler, E.; Zhu, Y.; Tour, J. M. *Nature* **2010**, *468*, 549−552.
(23) Biener, J.; Dasgupta, S.; Shao, L.; Wang, D.; Worsley, M. A.; Wittstock, A.; Lee, J. R. I.; Biener, M. M.; Orme, C. A.; Kucheyev, S. O.; Wood, B. C.; Willey, T. M.; Hamza, A. V.; Weissmüller, J.; Hahn, H.; Baumann, T. F. *Adv. Mater.* **2012**, *24*, 5083−5087.
(24) Lu, A. H.; Schüth, F. *Adv. Mater.* **2006**, *18*, 1793−1805.
(25) Fang, Y.; Lv, Y.; Che, R.; Wu, H.; Zhang, X.; Gu, D.; Zheng, G.; Zhao, D. *J. Am. Chem. Soc.* **2013**, *135*, 1524−1530.
(26) Macedo, J. S.; Otubo, L.; Ferreira, O. P.; Gimenez, I. d. F.; Mazali, I. O.; Barreto, L. S. *Microporous Mesoporous Mater.* **2008**, *107*, 276−285.
(27) Sevilla, M.; Fuertes, A. B. *Carbon* **2006**, *44*, 468−474.
(28) Deng, Y.; Liu, C.; Yu, T.; Liu, F.; Zhang, F.; Wan, Y.; Zhang, L.; Wang, C.; Tu, B.; Webley, P. A.; Wang, H.; Zhao, D. *Chem. Mater.* **2007**, *19*, 3271−3277.
(29) Xia, X.; Tu, J.; Mai, Y.; Chen, R.; Wang, X.; Gu, C.; Zhao, X. *Chem.−Eur. J.* **2011**, *17*, 10898−10905.
(30) Stankovich, S.; Dikin, D. A.; Piner, R. D.; Kohlhaas, K. A.; Kleinhammes, A.; Jia, Y.; Wu, Y.; Nguyen, S. T.; Ruoff, R. S. *Carbon* **2007**, *45*, 1558−1565.
(31) Huang, C.-h.; Doong, R.-a.; Gu, D.; Zhao, D. *Carbon* **2011**, *49*, 3055−3064.
(32) Gao, W.; Wan, Y.; Dou, Y.; Zhao, D. *Adv. Energy Mater.* **2011**, *1*, 115−123.
(33) Eda, G.; Chhowalla, M. *Adv. Mater.* **2010**, *22*, 2392−2415.
(34) Jung, I.; Dikin, D. A.; Piner, R. D.; Ruoff, R. S. *Nano Lett.* **2008**, *8*, 4283−4287.
(35) Hori, H.; Shikano, M.; Kobayashi, H.; Koike, S.; Sakaebe, H.; Saito, Y.; Tatsumi, K.; Yoshikawa, H.; Ikenaga, E. *J. Power Sources* **2013**, *242*, 844−847.

(36) Inamdar, A. I.; Kim, Y.; Pawar, S. M.; Kim, J. H.; Im, H.; Kim, H. *J. Power Sources* **2011**, *196*, 2393−2397.
(37) Xia, X. H.; Tu, J. P.; Zhang, J.; Wang, X. L.; Zhang, W. K.; Huang, H. *Sol. Energy Mater. Sol. Cells* **2008**, *92*, 628−633.
(38) Han, D.; Xu, P.; Jing, X.; Wang, J.; Yang, P.; Shen, Q.; Liu, J.; Song, D.; Gao, Z.; Zhang, M. *J. Power Sources* **2013**, *235*, 45−53.